

Simplifying multi-level thermal machines using virtual qubits

Ayaka Usui,^{1,*} Wolfgang Niedenzu,^{2,†} and Marcus Huber^{3,‡}

¹*Quantum Systems Unit, Okinawa Institute of Science and Technology Graduate University, Onna, Okinawa 904-0495, Japan*

²*Institut für Theoretische Physik, Universität Innsbruck, Technikerstraße 21a, A-6020 Innsbruck, Austria*

³*Institute for Quantum Optics and Quantum Information - IQOQI Vienna,
Austrian Academy of Sciences, Boltzmannngasse 3, 1090 Vienna, Austria*

(Dated: June 19, 2022)

Quantum thermodynamics often deals with the dynamics of small quantum machines interfacing with a large and complex environment. Virtual qubits, collisional models and reset master equations have become highly useful tools for predicting the qualitative behaviour of two-dimensional target systems coupled to few-qubit machines and a thermal environment. While matching the simplified model parameters for all possible physical systems is an impossibly hard task in general, the qualitative predictions still allow for a general design of quantum machines irrespective of the implementation. We generalise these tools by introducing multiple competing virtual qubits for modelling multi-dimensional systems coupled to larger and more complex machines. By simulating the full physical dynamics for targets with three dimensions, we uncover general properties of reset models that can be used as ‘dials’ to correctly predict the qualitative features of physical changes in a realistic setup and thus design autonomous quantum machines beyond a few qubits. We then present a general analytic solution of the reset model for arbitrary-dimensional systems coupled to multi-qubit machines. Finally, we showcase an improved three-level laser as an exemplary application of our results.

I. INTRODUCTION

Machines operating at the quantum scale offer an exploration of the ultimate limits of thermodynamic tasks [1–8], such as cooling down individual quantum systems or creating coherent sources of light. Design and control of such processes is usually assumed and achieved at the level of few quantum mechanical degrees of freedom, interacting with a large environment that one lacks detailed control over [9–14]. As large quantum systems are notoriously hard to simulate exactly, most of the focus is devoted on deriving master equations and dynamics for few-qubit machines or a single qutrit interacting with multiple baths. A crucial discovery in that context is the concept of a virtual qubit [15–17]. It allows to predict the steady state and even transient dynamics of a two-level transition of interest by focusing on the two levels that the transition effectively interacts with, which is called a virtual qubit. It dramatically reduces the complexity of predicting relevant machine behaviour, by sacrificing detailed knowledge of how the complex machine creating the virtual qubit behaves and shifts focus only on the target system of interest [18–21]. Going beyond simple qubit targets, however, is a challenge due to the potential complexity of competing interactions with multiple virtual qubits. In this paper, we solve the problem, for arbitrary-dimensional quantum systems (qudits), interacting with multiple competing virtual qubits across all possible two-level transitions in the context of reset-type master equations. We explore the solution for three-level

quantum systems and compare it to optical master equations, identifying a few universal features that these approaches share and thus important properties of complex machine designs that this simple and computable model correctly predicts. Finally, we use our model and analysis to study an enhancement of the paradigmatic three-level maser/laser [22] through more complex machines.

II. MOTIVATION: THE TWO-QUBIT MACHINE AS A VIRTUAL QUBIT

First, we review the idea of virtual qubits, which has been proposed in Ref. [15]. Consider two qubits with energy spacings Ω_1 and Ω_2 (we assume $\Omega_1 > \Omega_2$) that coherently interact with each other and are in contact with two thermal baths at temperatures T_1 and T_2 , respectively. This two-qubit machine is composed of the energy eigenstates $|0\rangle_1|0\rangle_2$, $|0\rangle_1|1\rangle_2$, $|1\rangle_1|0\rangle_2$, and $|1\rangle_1|1\rangle_2$. The single-excitation manifold is then called a *virtual qubit* whose ground and excited state are given by $|0\rangle_1|1\rangle_2$ and $|1\rangle_1|0\rangle_2$, respectively, with the energy spacing $\Omega_1 - \Omega_2$. The temperature of this virtual qubit, called the virtual temperature, is determined by the ratio between of the ground and excited state populations, which, together with the Boltzmann law, leads to

$$T_v = \frac{\Omega_1 - \Omega_2}{\Omega_1/T_1 - \Omega_2/T_2}. \quad (1)$$

Note that, since it is not a real temperature, T_v may be negative in the case of population inversion.

We now add another physical qubit, namely the *target qubit*, with energy spacing $\omega_1 - \omega_0 = \Omega_1 - \Omega_2$ that is coherently coupled to the two-qubit machine (see Fig. 1). Assuming that this target qubit is further interacting

* ayaka.usui@oist.jp

† Wolfgang.Niedenzu@uibk.ac.at

‡ marcus.huber@univie.ac.at

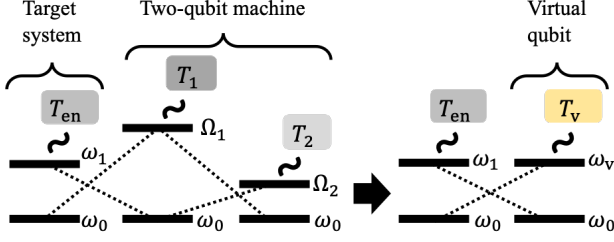


Figure 1. Sketch of a virtual qubit. Left: a target qubit coupled to a two-qubit machine, where $\omega_1 - \omega_0 = \Omega_1 - \Omega_2$. Right: the target qubit effectively coupled to a virtual qubit, where $\omega_v - \omega_0 = \Omega_1 - \Omega_2$ and T_v is given by Eq. (1). The dotted lines represent the coherent interactions given in Eq. (3). The wavy lines represent contact with baths whose temperatures are $T_{en,1,2}$.

with an environment at temperature T_{en} , the dynamics of the composite system are determined by the reset master equation (RME) [16, 17]

$$\begin{aligned} \frac{\partial \rho_{tot}}{\partial t} = & -i[H, \rho_{tot}] + Q_{en}(\tau_{en} \otimes \text{Tr}_{tar}[\rho_{tot}] - \rho_{tot}) \\ & + Q_1(\tau_1 \otimes \text{Tr}_1[\rho_{tot}] - \rho_{tot}) \\ & + Q_2(\tau_2 \otimes \text{Tr}_2[\rho_{tot}] - \rho_{tot}), \end{aligned} \quad (2)$$

where ρ_{tot} is the density matrix of the composite system. Here, $Q_{en,1,2}$ are thermalisation rates corresponding to the environment or the thermal baths in contact with the two-qubit machine, respectively. The density matrices $\tau_{en,1,2}$ are thermal states corresponding to the real temperatures $T_{en,1,2}$, respectively. The partial traces over the target qubit or the machine's constituents are denoted $\text{Tr}_{tar,1,2}$, respectively. The Hamiltonian in Eq. (2) reads

$$H = \sum_{k=0}^1 \omega_k |k\rangle\langle k| + \sum_{i \in \{1,2\}} \Omega_i \sigma_i^+ \sigma_i^- + g|0\rangle\langle 1| \sigma_1^+ \sigma_2^- + \text{H.c.} \quad (3)$$

with $\sigma_i^+ = |1\rangle_i \langle 0|_i$ and the coherent coupling strength g . Without the environment, the dynamics drive the target qubit into a steady state at the virtual temperature (1), independent of the rates Q_1 and Q_2 [15].

In general, however, the two-qubit machine is disturbed by the target qubit's interaction with the environment and hence the virtual temperature (1) is not the steady-state temperature anymore [17]. However, if the qubits inside the two-qubit machine thermalise very fast with the two baths at temperatures $T_{1,2}$, i.e., if $Q_{1,2} \gg Q_{en}, g$, the notion of the virtual temperature (1) remains valid.

Here, assuming $Q_{1,2} \gg Q_{en}, g$, we replace the two-qubit machine with a bath at the virtual temperature (1) and consider the effective reset master equation (efRME) for the target system only,

$$\frac{\partial \rho}{\partial t} = Q_{en}(\tau_{en} - \rho) + q_{vir}(\tau_{vir} - \rho), \quad (4)$$

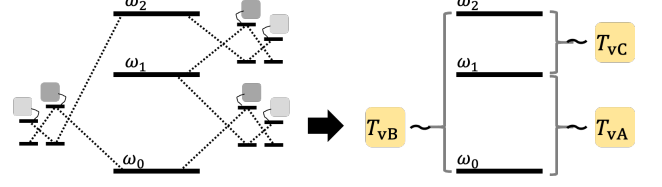


Figure 2. Simplification of two-qubit machines by using virtual qubits. Left: a qutrit coupled to three two-qubit machines. The dotted lines represent coherent interactions. Right: the qutrit where all the two-qubit machines are assumed to be baths at their virtual temperatures.

where q_{vir} is the effective thermalisation rate to the virtual qubit and τ_{vir} is a thermal state at the virtual temperature (1).

The steady-state solution of this effRME reads

$$\rho_{ss} = C(Q_{en}\tau_{en} + q_{vir}\tau_{vir}) \quad (5)$$

with the normalisation $C = (Q_{en} + q_{vir})^{-1}$. Note that owing to the two competitive dissipative couplings, this steady-state solution explicitly depends on the rates Q_{en} and q_{vir} .

Comparing this steady state (5) of the effRME with that from the RME (2), and using $Q_{1,2} \gg Q_{en}, g$, we find

$$q_{vir} = \frac{2g^2}{Q_1 + Q_2} (\tau_1^g \tau_2^e + \tau_1^e \tau_2^g). \quad (6)$$

Here, $\tau_{1,2}^{g,e}$ are the populations of the ground and excited states of the thermal state at temperatures $T_{1,2}$, respectively. We denote the *norm* of the virtual qubit

$$n_{vir} = \tau_1^g \tau_2^e + \tau_1^e \tau_2^g \quad (7)$$

as it corresponds to the weight of the levels $|0\rangle_1 |1\rangle_2$ and $|1\rangle_1 |0\rangle_2$ that form the virtual qubit within the two-qubit machine space. This norm thus determines the temperature dependence of the effective rate q_{vir} .

III. THREE-LEVEL SYSTEM COUPLED TO THREE TWO-LEVEL MACHINES

We now continue by applying the idea of virtual qubits to higher-dimensional target systems. In this section, we consider a three-level system, i.e., a qutrit, with energy spacings $\omega_{0,1,2}$ that is coupled to several two-qubit machines (Fig. 2). Within the effRME description, each of these two-qubit machines is regarded as a virtual qubit.

With a single machine coupled to the target qutrit, the situation is essentially the same as the qubit target shown Fig. 1. With two machines coupled, two distinct thermalisation processes act on the target. Consequently, the steady state of the latter is not a Gibbs-like state, unless both virtual temperatures are the same. As an example, if a machine with virtual temperature T_{v1} is connected to the target levels $|0\rangle$ and $|1\rangle$ and another one

with virtual temperature T_{v2} is connected to the levels of $|0\rangle$ and $|2\rangle$, the qutrit is driven into the steady state

$$\rho_{ss} = C \left(|0\rangle\langle 0| + e^{-(\omega_1 - \omega_0)/T_{v1}} |1\rangle\langle 1| + e^{-(\omega_2 - \omega_0)/T_{v2}} |2\rangle\langle 2| \right) \quad (8)$$

with the normalisation $C = (1 + e^{-(\omega_1 - \omega_0)/T_{v1}} + e^{-(\omega_2 - \omega_0)/T_{v2}})^{-1}$. As the two thermalisation processes do not compete, each transition is “thermalised” to its respective virtual temperature T_{v1}, T_{v2} . By contrast, if all transitions within the target qutrit interact with independent two-level machines (see Fig. 2), the three thermalisation process compete against each other unless all the virtual temperatures are equal.

Below, we utilise the idea of the virtual qubits to construct an effRME of the three-level target system as we did for the qubit target system. To explore the parameter dependency of the effective thermalisation rates, we compare the steady state among the effRME for the target system and two non-exclusive physical models for the corresponding machine setup: the full RME for target plus machine and an optical master equation, i.e., a so-called Gorini-Kossakowski-Lindblad-Sudarshan master equation (GKLSME). Finally, we discuss these models’ relations to the effRME.

III.1. Effective reset master equation (effRME)

We consider a qutrit coherently coupled to three pairs of two physical qubits, as depicted in Fig. 2. We label as “A” the pair coupled to the levels of $|0\rangle$ and $|1\rangle$, as “B” the pair coupled to the levels of $|0\rangle$ and $|2\rangle$, and as “C” the pair coupled to the levels of $|1\rangle$ and $|2\rangle$. Each of the pairs has two qubits with energy spacings Ω_{i1} and Ω_{i2} , and the qubits are in contact with baths of which temperatures are T_{i1} and T_{i2} , respectively, for $i \in \{A, B, C\}$. Furthermore, due to energy conservation, the energy spacings are restricted as $\omega_1 - \omega_0 = \Omega_{A1} - \Omega_{A2}$, $\omega_2 - \omega_0 = \Omega_{B1} - \Omega_{B2}$, and $\omega_2 - \omega_1 = \Omega_{C1} - \Omega_{C2}$.

We assume that the thermalisation of the qubits inside the two-qubit machines is fast enough that the concept of the virtual temperature is valid. By considering that the two-qubit machines maintain their virtual temperatures, the effRME of the target system is provided by

$$\frac{\partial \rho}{\partial t} = \sum_{i \in \{A, B, C\}} q_i (\tau_i \otimes \text{Tr}_i[\rho] - \rho), \quad (9)$$

where $q_{A,B,C}$ are the effective thermalisation rates and $\text{Tr}_{A,B,C}$ represent tracing out the space of the qubit pairs A, B, C, respectively. The states $\tau_{A,B,C}$ are thermal states at the virtual temperatures T_{vA}, T_{vB}, T_{vC} , respectively, given by

$$T_{vi} = \frac{\Omega_{i1} - \Omega_{i2}}{\Omega_{i1}/T_{i1} - \Omega_{i2}/T_{i2}} \quad (10)$$

for $i \in \{A, B, C\}$. Explicitly, these states read $\tau_A = \tau_A^g |0\rangle\langle 0| + \tau_A^e |1\rangle\langle 1|$, $\tau_B = \tau_B^g |0\rangle\langle 0| + \tau_B^e |2\rangle\langle 2|$, and $\tau_C = \tau_C^g |1\rangle\langle 1| +$

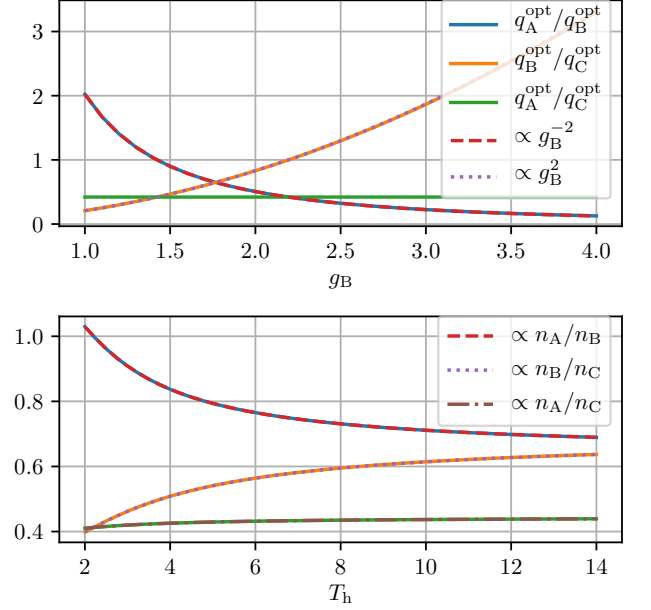


Figure 3. Optimal coupling coefficient rates between the target qutrit and the auxiliary qubits for which the state (11) is the steady-state solution of the RME (13) as a function of coherent interaction strength g_B (upper panel) and bath temperature $T_{i1} = T_h$ (lower panel). In the upper panel, the ratio q_A/q_B is proportional to $1/g_B^2$, and the ratio q_B/q_C is proportional to g_B^2 . In the lower panel, the ratios q_i/q_j are proportional to the ratios n_i/n_j of the norms (15) of the virtual qubits for $i, j \in \{A, B, C\}$. Both plots use the same parameter set, except for $T_{i1} = T_h = 3.1$ in the upper panel and $g_B = 1.5$ in the lower panel. Apart from the two parameters, the following is used: $\omega_0 = 0$, $\omega_1 = 2$, $\omega_2 = 3$, $\Omega_{A1} = 2.5$, $\Omega_{B1} = 4.5$, $\Omega_{C1} = 1.3$, $g_A = 1.2$, $g_C = 1.8$, $T_{i1} = T_h = 3.1$, $T_{i2} = T_c = 1.2$, $Q_{i1} = 70$, and $Q_{i2} = 50$ for $i \in \{A, B, C\}$.

$\tau_C^e |2\rangle\langle 2|$, respectively, where $\tau_i^{g,e}$ are the respective populations of the ground and excited states. By solving the effRME (9) for $\partial \rho / \partial t = 0$, the steady state of the target system can be found as

$$\rho_{ss} = C (q_A q_B \tau_{AB} + q_B q_C \tau_{BC} + q_C q_A \tau_{CA}), \quad (11)$$

where the normalisation is $C = (q_A q_B \text{Tr}[\tau_{AB}] + q_B q_C \text{Tr}[\tau_{BC}] + q_C q_A \text{Tr}[\tau_{CA}])^{-1}$. The steady state (11) is thus a combination of the respective steady states if only two of the three coherent couplings are present, i.e.,

$$\tau_{AB} = \tau_A^g \tau_B^g |0\rangle\langle 0| + \tau_A^e \tau_B^g |1\rangle\langle 1| + \tau_A^g \tau_B^e |2\rangle\langle 2|, \quad (12a)$$

$$\tau_{BC} = \tau_B^g \tau_C^g |0\rangle\langle 0| + \tau_B^e \tau_C^g |1\rangle\langle 1| + \tau_B^g \tau_C^e |2\rangle\langle 2|, \quad (12b)$$

$$\tau_{CA} = \tau_C^g \tau_A^g |0\rangle\langle 0| + \tau_C^e \tau_A^g |1\rangle\langle 1| + \tau_C^g \tau_A^e |2\rangle\langle 2|. \quad (12c)$$

Note that these states are not normalised on purpose, i.e., $\text{Tr}[\tau_{AB}] \neq 1$, $\text{Tr}[\tau_{BC}] \neq 1$, and $\text{Tr}[\tau_{CA}] \neq 1$.

We have generalised this virtual-qubit treatment to n -dimensional target systems in Appendix A and discuss the steady-state solution of four-dimensional target systems in Appendix B.

III.2. Reset master equation (RME)

Here, we present the REM for the composite system (target and machine) and compare its steady state with the steady state (11) of the effRME. The RME describing the composite system reads

$$\frac{\partial \rho_{\text{tot}}}{\partial t} = -i[H, \rho_{\text{tot}}] + \sum_{i \in \mathcal{I}} Q_i (\tau_i \otimes \text{Tr}_i[\rho_{\text{tot}}] - \rho_{\text{tot}}), \quad (13)$$

with the respective thermalisation rates Q_i for $\mathcal{I} := \{A1, A2, B1, B2, C1, C2\}$. The Hamiltonian is given by

$$H = \sum_{k=0}^2 \omega_k |k\rangle\langle k| + \sum_{i \in \mathcal{I}} \Omega_i \sigma_i^+ \sigma_i^- + [g_A |0\rangle\langle 1| \sigma_{A1}^+ \sigma_{A2}^- + g_B |0\rangle\langle 2| \sigma_{B1}^+ \sigma_{B2}^- + g_C |1\rangle\langle 2| \sigma_{C1}^+ \sigma_{C2}^- + \text{H.c.}] \quad (14)$$

with the coupling strengths $g_{A,B,C}$ to each of the subsystems and the qubit frequencies $\Omega_{A2} := \Omega_{A1} - (\omega_1 - \omega_0)$, $\Omega_{B2} := \Omega_{B1} - (\omega_2 - \omega_0)$, $\Omega_{C2} := \Omega_{C1} - (\omega_2 - \omega_1)$. While the solution of $\partial \rho_{\text{tot}} / \partial t = 0$ provides the steady state of the composite system, solving this equation analytically is difficult due to the size of the system, which is $3 \times 2^2 \times 2^2 \times 2^2 = 192$. Even if numerical solutions of $\partial \rho_{\text{tot}} / \partial t = 0$ are obtained, it is hard to understand what the steady state shows physically and what kind of parameters characterise the steady state in contrast to the effRME.

In order to characterise the effective thermalisation rates $q_{A,B,C}$ in the effRME, we compute the steady-state solution of the RME (13). Here, $\omega_0 = 0$ is taken, and the energy unit is set as half of the energy gap between the ground and first excited states of the qutrit, $(\omega_1 - \omega_0)/2 = \omega_1/2 = 1$. Also, our focus is on a regime where the thermalisation rates $\{Q_i\}$ are much larger than any other energy scales such that the virtual temperatures are still valid. By finding the population at each level in the RME solution corresponding to that in the effRME solution (11), we have obtained the parameter dependency of the effective thermalisation rates $q_{A,B,C}$. Assuming that all the two-qubit machines are subject to the same bath temperatures, i.e., $T_{i1} = T_h$ and $T_{i2} = T_c$ for $i \in \{A, B, C\}$, we plot the ratio of the effective thermalisation rates $q_{A,B,C}$ as a function of the coherent coupling strength g_B and the hot bath temperature T_h in Fig. 3. It is seen that the ratio q_i/q_j is proportional to g_i^2/g_j^2 and that the T_h -dependency of the ratio q_i/q_j corresponds to the norm of virtual qubits, which, in analogy to Eq. (7), reads

$$n_i = \tau_{i1}^g \tau_{i2}^c + \tau_{i1}^c \tau_{i2}^g \quad (15)$$

for $i \in \{A, B, C\}$. These parameter dependencies are consistent with the effective thermalisation rate (6) in the case of a two-dimensional target system.

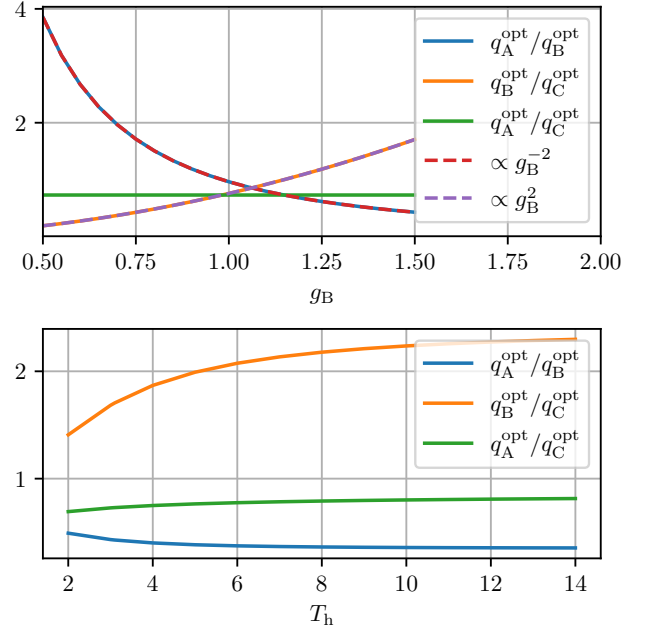


Figure 4. Optimal rates of the effRME (9) for which the state (11) is the steady-state solution of the GKLSME (16) as a function of the coherent coupling strength g_B (upper panel) and the hot-bath temperature T_h (lower panel). The quadratic relation (18) can clearly be seen in the upper panel. While $T_h = 3.1$ is used in the upper panel and $g_B = 1.5$ is used in the lower panel, both of the panels use the same values for the other parameters: $\omega_0 = 0$, $\omega_1 = 2$, $\omega_2 = 3$, $g_A = 1.2$, $g_C = 1.8$, $\Omega_{A1} = 2.5$, $\Omega_{B1} = 4.5$, $\Omega_{C1} = 1.3$, $T_c = 1.2$, $t = 10$, $\Gamma_{i1} = 70$, and $\Gamma_{i2} = 50$ for $i \in \{A, B, C\}$.

III.3. Gorini-Kossakowski-Lindblad-Sudarshan master equation (GKLSME)

We now continue to focus on the case of the target system being a qutrit. The idea of virtual qubits is then to replace the “full” RME (13) that governs the dynamics of the joint system composed of the target qutrit and the six physical qubits (with the coupling rates Q_i) by an effRME that contains fewer “virtual” qubits (with the rates q_i). Namely, Eq. (13) is replaced by Eq. (9). The mapping of the rates, $\{Q_i\} \mapsto \{q_i\}$, is, in general, intricate. Notwithstanding, for the case of a target qubit we found that some features of the analytic relation (6), such as the dependence on the coherent Hamiltonian coupling g_i and the dependence on the norms, are numerically reproduced for a target qutrit in the foregoing section.

The description of the physical system that underlies the effRME (9) is not unique and may depend on the concrete physical setup. In a sense, the RME (13) constitutes, by itself, also an ad-hoc model, as it is not based on some continuous interaction with the environment, but a stochastic full swapping of constituent states with environment states. Nonetheless, owing to its CPTP (completely positive and trace-preserving) behaviour, the

RME may be cast into a GKLSME, known from conventional thermalisation models [23–25]. This mapping is, in general, a complicated function of the physical parameters, such as the bath temperatures, and has been explicitly derived for special cases [26]. There, it is shown that in order to fulfil the mapping, the spontaneous emission rates Γ_i in the GKLSME (see below) must be temperature-dependent, which is a feature that is usually not encountered in GKLSMEs [25].

On the other hand, we may have also chosen to formulate the original system in terms of a GKLSME with independent rates Γ_i and then map it onto a “full” RME. Thereby, the rates Q_i of the latter become themselves functions of the system parameters. As a consequence, the temperature dependence of the effective rates q_i in the effRME for the target only is expected to depend on more than just the norms of the virtual qubits. The question of which description is more favourable depends on what parameters are easily tunable in a concrete experimental scenario. We will come back to this distinction in the next section and here assume the GKLSME to be the original equation and strive to understand the behaviour of q_i in dependence of the physical parameters.

The GKLSME for a target qutrit that interacts with six physical qubits reads

$$\frac{\partial \rho_{\text{tot}}}{\partial t} = -i[H, \rho_{\text{tot}}] + \sum_{i \in \mathcal{I}} \mathcal{L}_i \rho_{\text{tot}}, \quad (16)$$

with the Hamiltonian (14) and the qubits $\mathcal{I} = \{A1, A2, B1, B2, C1, C2\}$. The Liouvillian

$$\mathcal{L}_i \rho = \Gamma_i (\bar{n}(\Omega_i, T_i) + 1) \mathcal{D}[\sigma_i^-] + \Gamma_i \bar{n}(\Omega_i, T_i) \mathcal{D}[\sigma_i^+] \quad (17)$$

describes the dissipative interaction of the i th auxiliary qubit with its bath (see also Fig. 1) at temperature $T_i = T_h$ for $i \in \{A1, B1, C1\}$ and $T_i = T_c$ for $i \in \{A2, B2, C2\}$, respectively; Γ_i is that qubit’s spontaneous emission rate. We have further defined the thermal population $\bar{n}(\omega, T) := [\exp(\omega/T) - 1]^{-1}$ of the bosonic bath and the dissipator $D[A] := 2A\rho A^\dagger - A^\dagger A\rho - \rho A^\dagger A$.

We now replace this equation with the simple effRME (9) for the qutrit only and pose the question: How are the parameters $\{q_A, q_B, q_C\}$ of the effRME (9) related to the parameters of the GKLSME (16)? To answer this question, we numerically integrate the GKLSME (16) for given parameters with the analytic steady-state solution (11), which is parameterised by the triple (q_A, q_B, q_C) , as the initial state of the target qutrit (the qubits were initialised to their respective thermal states). We repeat this integration for different such triples to minimise the Frobenius norm $\|\rho(t) - \rho(0)\|$ between the reduced density operators of the qutrit at time t and time $t = 0$ for a sufficiently large fixed time $t > 0$. The Frobenius norm thus quantifies the deviation of the time-evolved state to the initial state (11). Thereby, we find the optimal parameter triple $(q_A^{\text{opt}}, q_B^{\text{opt}}, q_C^{\text{opt}})$ for which Eq. (11) is the steady-state solution of Eq. (16). By repeating this procedure for, e.g., different T_h , we can then

numerically find the dependence of the rates q_i on the physical parameters of the GKLSME (see Fig. 4).

As seen from the upper panel in Fig. 4, the quadratic relation

$$\frac{q_i^{\text{opt}}}{q_j^{\text{opt}}} \propto \frac{g_i^2}{g_j^2} \text{ for } i, j \in \{A, B, C\} \quad (18)$$

of the effective rates in the effRME (9) to the Hamiltonian couplings in the GKLSME (16), first obtained in Eq. (6) for the qubit case, is reproduced, but with different proportionality factors than in Fig. 3. Whilst we only show the dependence on g_B in Fig. 4, we have performed additional simulations for varying g_A and g_C , respectively, that are fully consistent with the quadratic behaviour in Eq. (18). Furthermore, as expected, the temperature dependence does not agree with the norm of the virtual qubits (see the lower panel in Fig. 4), which will be discussed more in the next section.

We have implemented these simulations with the QuantumOptics.jl [27] Julia framework and used Optim.jl [28] for the numerical optimisation procedure.

III.4. Discussion and identifying the “dials”

Our setup possesses a plethora of parameters, and the question on how they influence the steady-state solution of the target qutrit is not trivial. What we have seen above is that the behaviour of the optimal q_i^{opt} as a function of, e.g., the hot-bath temperature T_h differs, depending on the description: Whereas in the case of the reset model, the ratios of the q_i^{opt} depend on the corresponding ratio of the norms (15) of the virtual qubits, this is not the case in the GKLS treatment.

To understand this issue, it is important to note that in the RME for the seven-body system (target qutrit and six qubits) the parameters Q_i were assumed to be *independent* of the temperature. Therefore, the only temperature dependence in the q_i^{opt} stems from the norm. The GKLSME equivalent to the RME possesses temperature-dependent spontaneous emission rates. By contrast, in Sec. III.3 we have considered rates that do not depend on the temperatures. Therefore, the temperature dependence in Figs. 3 and 4 differ.

It is important to note that although the RME can be written in GKLS form, the latter will not depict the behaviour that we are accustomed to from typical quantum-optical situations: Usually, the decay rates Γ_i do not depend on the temperatures [25], but the rates in the GKLS form of the reset equation will do, similar to Ref. [26]. Therefore, features such as the temperature difference of the steady-state solution strongly depend on whether the Q_i or the Γ_i are assumed to be “auxiliary” parameters with no further dependence on the temperatures. If the Q_i are deemed to be independent, then the Γ_i will depend on the temperatures. Conversely, if the Γ_i are chosen to be independent, then the Q_i will depict a temperature

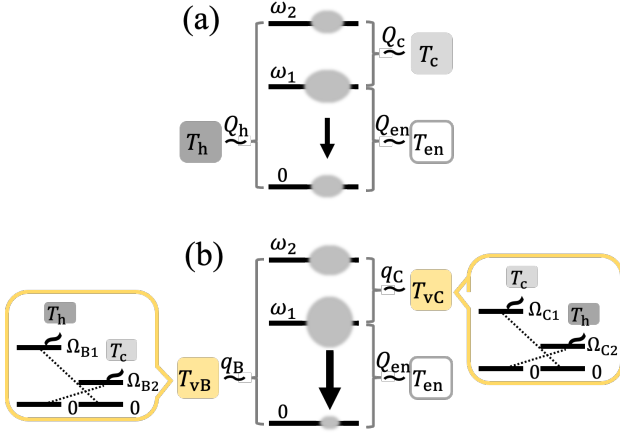


Figure 5. Sketches of (a) a typical laser mechanism with T_h the hot-bath temperature and T_c the cold-bath temperature, and (b) our proposed scheme improved by virtual temperatures, where T_{vB} [Eq. (19)] is negative and T_{vC} [Eq. (20)] is smaller than T_c . The oval on each qutrit level represents this level's population. The lasing transition is further coupled to an environment at temperature T_{en} .

dependence and would not correspond to the ratio of the norms anymore as shown in the lower panel in Fig. 4. We note that although the Γ_i in the GKLS description typically depend on the frequencies [25], we may still see them as independent parameters since the frequency dependence may be countered by, e.g., changing the dipole moment of the qubit. It is therefore sensible to assume the rates to be “auxiliary” parameters in either description (although the concrete parameter dependence of the ad-hoc Q_i may be unknown). By contrast, the features that only depend on the Hamiltonian part of the master equation coincide in both descriptions, cf. the quadratic dependence on g_B in Figs. 3 and 4, although the proportionality factors differ.

It is therefore of paramount importance to distinguish between the two genuinely different models

- RME with “free” Q_i
- GKLSME with “free” Γ_i

and the mapping of the RME to a GKLSME and vice versa, where the “free” character of the rates no longer holds. The “dials” therefore very much depend on the initial description of the machine, i.e., whether the Q_i or the Γ_i are supposed to be tunable by some auxiliary parameters. Both physical models, RME and GKLSME, therefore have their respective merit in different (experimental) setups.

IV. EXAMPLE: IMPROVING A LASER WITH POPULATION INVERSION

As an exemplary application of our method, we propose a scheme to enhance the output of a three-level laser

by coupling it to a complex machine. A typical lasing mechanism [22, 29, 30] is shown in Fig. 5(a). The laser is composed of a three-level system in contact with a hot bath at temperature T_h and a cold bath at T_c that above the lasing threshold creates a population inversion between the lasing levels $|0\rangle$ and $|1\rangle$. In the following we pose the question: Can this population inversion be increased by indirectly coupling this three-level system to those temperatures via auxiliary two-qubit machines [Fig. 5(b)]? Namely, we replace the hot bath with a two-qubit machine whose virtual temperature T_{vB} is [cf. Eq. (10)]

$$T_{vB} = \frac{\Omega_{B1} - \Omega_{B2}}{\Omega_{B1}/T_h - \Omega_{B2}/T_c}, \quad (19)$$

where $\Omega_{B2} = \Omega_{B1} - (\omega_2 - \omega_0)$. Note that for a fair comparison, the hot- and cold-bath temperatures used for the laser are also applied to this two-qubit machine. For $T_h > (\Omega_{B1}/\Omega_{B2})T_c$, the virtual temperature T_{vB} is negative and leads to population inversion between the levels $|0\rangle$ than $|2\rangle$ [see Fig. 5(b)]. Larger population in a higher energy state than a lower energy state is never seen with real thermal baths. This population inversion between the levels $|0\rangle$ and $|2\rangle$ therefore increases the desired inversion on the lasing transition between $|0\rangle$ and $|1\rangle$ and hence increases the performance of the laser.

The inversion on the lasing transition can be further improved by replacing the cold bath by a virtual qubit at the virtual temperature

$$T_{vC} = \frac{\Omega_{C1} - \Omega_{C2}}{\Omega_{C1}/T_c - \Omega_{C2}/T_h}. \quad (20)$$

Since $T_h > T_c$ and $\Omega_{C2} = \Omega_{C1} - (\omega_2 - \omega_1)$, T_{vC} is always lower than T_c .

Hence, our proposed scheme works better than the typical laser for $T_h > (\Omega_{B1}/\Omega_{B2})T_c$ since the population inversion can be increased. This can be seen in Fig. 6, where we plot the population ratio p_1/p_0 as a function of T_h . For the ideal, i.e., lossless, case where the lasing transition is not subject to any additional environment, the optimal population inversion is realised if $T_{vB} \rightarrow -\infty$ and $T_{vC} \rightarrow 0$. For fixed bath temperatures, this could, e.g., be achieved by tuning the respective energy spacings Ω_{B1} and Ω_{C1} within the two-qubit machines.

For a more realistic situation with photon losses through an additional environment at temperature T_{en} that interacts with the lasing transition, the additional coupling Q_{en} competes with the rates to the virtual qubits. Namely, the steady state of the three-level system explicitly depends on those rates, and therefore the optimal virtual temperatures are no longer the same as the ideal lossless case. In analogy to Eq. (11), the steady state of the target qutrit reads

$$\rho_{ss} \propto (Q_{en} q_B \tau_{enB} + q_B q_C \tau_{BC} + q_C Q_{en} \tau_{Cen}), \quad (21)$$

where the states $\tau_{enB,BC,Cen}$ are determined in analogy to Eqs. (12). As seen in Figs. 3 and 4, the rates $q_{B,C}$

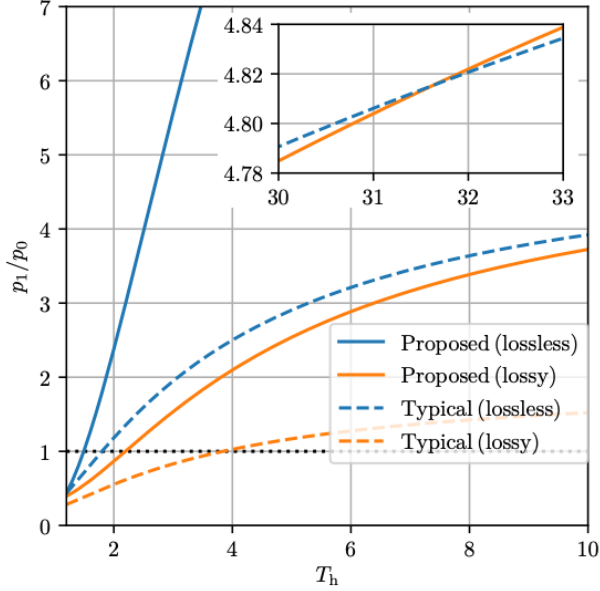


Figure 6. Population ratio p_1/p_0 of the levels $|0\rangle$ and $|1\rangle$ of the qutrit in the typical laser and in our scheme when changing the hot temperature T_h . The population ratio p_1/p_0 is displayed in cases of the typical laser (directly coupled to the heat baths) and our proposed scheme (indirectly coupled to the baths via two-qubit machines that give rise to virtual temperatures) with and without photon loss. The dotted black line represents the lasing threshold $p_1/p_0 = 1$. “Lossless” (“lossy”) means no (non-zero) photon loss. The inset zooms in on a regime that our proposed scheme with photon loss considered outperforms the lossless typical laser. The bath temperature and the thermalisation rate associated with loss of the laser output are assumed to be $T_{\text{en}} = 7.2$ and $Q_{\text{en}} = 0.1$. For the actual thermalisation rates, $Q_h = 2$ and $Q_c = 1.5$ are taken. The other parameters are the same as Figs. 3 and 4: $\omega_0 = 0$, $\omega_1 = 2$, $\omega_2 = 3$, $\Omega_{B1} = 4.5$, $\Omega_{C1} = 1.3$, $T_c = 1.2$.

depend on the machine parameters. Therefore, these rates also change while tuning the bath temperatures $T_{h,c}$ to control the virtual temperatures $T_{vB,vC}$. By contrast, for the typical heat-pumped three-level laser, where the target is directly coupled to the thermal baths, the target relaxes to

$$\rho_{\text{ss}} \propto (Q_{\text{en}} Q_h \tau_{\text{enh}} + Q_h Q_c \tau_{\text{hc}} + Q_c Q_{\text{en}} \tau_{\text{cen}}), \quad (22)$$

where the states $\tau_{\text{enh,hc,cen}}$ are also obtained in analogy to Eqs. (12).

To demonstrate that our proposed scheme can still outperform the typical three-level laser even in the non-ideal, lossy, case, we show the dependence of the population ratios p_1/p_0 obtained from Eq. (21) and Eq. (22), respectively, as a function of the hot-bath temperature in Fig. 6. To this end, we chose fixed values for the couplings Q_h , Q_c and Q_{en} and set the effective rates to be

$$q_B = Q_h n_B, \quad (23a)$$

$$q_C = Q_c n_C, \quad (23b)$$

with the norms (15) to allow for a fair comparison between the two laser setups in Fig. 5. Namely, we assume the internal details of the two-qubit machines [yellow boxes in Fig. 5(b)] to be tuned in such a way that the effective rates are Eqs. (23). It is seen in Fig. 6 that using the more complex setup with virtual qubits the population inversion of the lasing transition can be strongly increased. For the chosen parameters, our scheme allowing for photon loss outperforms even the typical laser outcome in the ideal case for $T_h \gtrsim 32$ (see the inset in Fig. 6). Note that we only tune T_h and leave the other parameters such as the qubit frequencies invariant. If one tunes the other parameters as well, the lasing transition can be improved efficiently.

V. CONCLUSIONS

Designing complex thermal machines at the quantum scale is hard, as they quickly become intractable. We have instead decided to model only the steady state of an arbitrary-dimensional target system in contact with a complex machinery coupled to different heat baths. This can be done by means of competing virtual qubits, coupled to the different transitions of the quantum target. Using reset-type master equations, this enables an analytical solution for all dimensions. We have studied and showcased the behaviour in three dimension, comparing it to full solutions of an optical master equation (GKLSME) and showed that they share central features and behaviours, whereas the exact target state can at times be different. The models are nonetheless useful for designing machines to optimise certain key properties of the target system, such as inverting the population of the lasing transition in a three-level laser, or generally to optimally create purity in a subspace of the multi-level system.

ACKNOWLEDGMENTS

A. U. acknowledges support from IQOQI-Vienna for visiting, financial support from OIST Graduate University, Research Fellowship of JSPS for Young Scientists, and JSPS KAKENHI Grant Number 20J10006. W. N. acknowledges support from an ESQ fellowship of the Austrian Academy of Sciences (ÖAW). M. H. also acknowledges funds from the FQXi (FQXi-IAF19-03-S2) within the project “*Fueling quantum field machines with information*” and from the Austrian Science Fund (FWF) through the START project Y879-N27. All authors acknowledge productive discussions with the QUIT physics group and useful comments on the manuscript from Thomas Busch.

- [1] R. Alicki, The quantum open system as a model of the heat engine, *J. Phys. A* **12**, L103 (1979).
- [2] R. Kosloff, A quantum mechanical open system as a model of a heat engine, *J. Chem. Phys.* **80**, 1625 (1984).
- [3] R. Kosloff, Quantum Thermodynamics: A Dynamical Viewpoint, *Entropy* **15**, 2100 (2013).
- [4] D. Gelbwaser-Klimovsky, W. Niedenzu, and G. Kurizki, Thermodynamics of Quantum Systems Under Dynamical Control, *Adv. At. Mol. Opt. Phys.* **64**, 329 (2015).
- [5] J. Goold, M. Huber, A. Riera, L. del Rio, and P. Skrzypczyk, The role of quantum information in thermodynamics—a topical review, *J. Phys. A* **49**, 143001 (2016).
- [6] S. Vinjanampathy and J. Anders, Quantum thermodynamics, *Contemp. Phys.* **57**, 545 (2016).
- [7] A. Ghosh, W. Niedenzu, V. Mukherjee, and G. Kurizki, Thermodynamic Principles and Implementations of Quantum Machines, in *Thermodynamics in the Quantum Regime*, edited by F. Binder, L. A. Correa, C. Gogolin, J. Anders, and G. Adesso (Springer, Cham, 2019) pp. 37–66.
- [8] S. Bhattacharjee and A. Dutta, Quantum thermal machines and batteries, *arXiv preprint arXiv:2008.07889* (2020).
- [9] J. V. Koski, V. F. Maisi, J. P. Pekola, and D. V. Averin, Experimental realization of a Szilard engine with a single electron, *Proc. Natl. Acad. Sci. USA* **111**, 13786 (2014).
- [10] J. Roßnagel, S. T. Dawkins, K. N. Tolazzi, O. Abah, E. Lutz, F. Schmidt-Kaler, and K. Singer, A single-atom heat engine, *Science* **352**, 325 (2016).
- [11] J. Klaers, S. Faelt, A. Imamoglu, and E. Togan, Squeezed Thermal Reservoirs as a Resource for a Nanomechanical Engine beyond the Carnot Limit, *Phys. Rev. X* **7**, 031044 (2017).
- [12] J. P. S. Peterson, T. B. Batalhão, M. Herrera, A. M. Souza, R. S. Sarthour, I. S. Oliveira, and R. M. Serra, Experimental Characterization of a Spin Quantum Heat Engine, *Phys. Rev. Lett.* **123**, 240601 (2019).
- [13] D. von Lindenfels, O. Gräß, C. T. Schmiegelow, V. Kaushal, J. Schulz, M. T. Mitchison, J. Goold, F. Schmidt-Kaler, and U. G. Poschinger, Spin Heat Engine Coupled to a Harmonic-Oscillator Flywheel, *Phys. Rev. Lett.* **123**, 080602 (2019).
- [14] J. Klatzow, J. N. Becker, P. M. Ledingham, C. Weinzel, K. T. Kaczmarek, D. J. Saunders, J. Nunn, I. A. Walmsley, R. Uzdin, and E. Poem, Experimental Demonstration of Quantum Effects in the Operation of Microscopic Heat Engines, *Phys. Rev. Lett.* **122**, 110601 (2019).
- [15] N. Brunner, N. Linden, S. Popescu, and P. Skrzypczyk, Virtual qubits, virtual temperatures, and the foundations of thermodynamics, *Phys. Rev. E* **85**, 051117 (2012).
- [16] N. Linden, S. Popescu, and P. Skrzypczyk, How Small Can Thermal Machines Be? The Smallest Possible Refrigerator, *Phys. Rev. Lett.* **105**, 130401 (2010).
- [17] P. Skrzypczyk, N. Brunner, N. Linden, and S. Popescu, The smallest refrigerators can reach maximal efficiency, *J. Phys. A: Math. Theor.* **44**, 492002 (2011).
- [18] R. Silva, G. Manzano, P. Skrzypczyk, and N. Brunner, Performance of autonomous quantum thermal machines: Hilbert space dimension as a thermodynamical resource, *Phys. Rev. E* **94**, 032120 (2016).
- [19] P. Erker, M. T. Mitchison, R. Silva, M. P. Woods, N. Brunner, and M. Huber, Autonomous Quantum Clocks: Does Thermodynamics Limit Our Ability to Measure Time? *Phys. Rev. X* **7**, 031022 (2017).
- [20] S. Seah, S. Nimmrichter, and V. Scarani, Refrigeration beyond weak internal coupling, *Phys. Rev. E* **98**, 012131 (2018).
- [21] G. Manzano, R. Silva, and J. M. R. Parrondo, Autonomous thermal machine for amplification and control of energetic coherence, *Phys. Rev. E* **99**, 042135 (2019).
- [22] H. E. D. Scovil and E. O. Schulz-DuBois, Three-Level Masers as Heat Engines, *Phys. Rev. Lett.* **2**, 262 (1959).
- [23] G. Lindblad, On the generators of quantum dynamical semigroups, *Commun. Math. Phys.* **48**, 119 (1976).
- [24] V. Gorini, A. Kossakowski, and E. C. G. Sudarshan, Completely positive dynamical semigroups of N-level systems, *J. Math. Phys.* **17**, 821 (1976).
- [25] H.-P. Breuer and F. Petruccione, *The Theory of Open Quantum Systems* (Oxford University Press, Oxford, 2002).
- [26] A. Tavakoli, G. Haack, M. Huber, N. Brunner, and J. B. Brask, Heralded generation of maximal entanglement in any dimension via incoherent coupling to thermal baths, *Quantum* **2**, 73 (2018).
- [27] S. Krämer, D. Plankensteiner, L. Ostermann, and H. Ritsch, QuantumOptics.jl: A Julia framework for simulating open quantum systems, *Comput. Phys. Commun.* **227**, 109 (2018).
- [28] P. K. Mogensen and A. N. Riseth, Optim: A mathematical optimization package for Julia, *J. Open Source Softw.* **3**, 615 (2018).
- [29] E. Boukobza and D. J. Tannor, Three-Level Systems as Amplifiers and Attenuators: A Thermodynamic Analysis, *Phys. Rev. Lett.* **98**, 240601 (2007).
- [30] W. Niedenzu, M. Huber, and E. Boukobza, Concepts of work in autonomous quantum heat engines, *Quantum* **3**, 195 (2019).

Appendix A: Steady-state solution of effRME for n -level target system

We discuss the steady-state solution for an effRME in a multi-level system with some two-qubit machines coupled. For simplicity, let us adhere to cases where every pair of levels in the target is coupled to one machine. In these cases, for n -level systems the number of the couplings is $\binom{n}{2} = n(n-1)/2$.

We generalise the effRME to n -level target systems. For distinct representation, let us introduce different notation of coupling strength from that in Fig. 2. We write $q_{k,l}$ as the thermalisation rate of the k th and l th levels ($k < l$), where the indices A, B, C in Fig. 2 are associated with $q_{0,1}$, $q_{0,2}$, and $q_{1,2}$, respectively. The effRME for n -level target system is written as

$$\frac{\partial \rho}{\partial t} = \sum_{l=1}^{n-1} \sum_{k=0}^{l-1} q_{k,l} (\tau_{k,l} \otimes \text{Tr}_{k,l}[\rho] - \rho), \quad (\text{A1})$$

where $\tau_{k,l}$ is a thermal state at the virtual temperature associated with the k th and l th levels, and $\text{Tr}_{k,l}$ represents tracing out the space of the k th and l th levels. We ignore off-diagonal terms in the density matrix since in this model coherence cannot be generated. Then, this equation can be simplified as

$$\frac{\partial \rho}{\partial t} = \sum_{l=1}^{n-1} \sum_{k=0}^{l-1} q_{k,l} \left(-\tau_{k,l}^e \rho^{(k)} + \tau_{k,l}^g \rho^{(l)} \right) (|k\rangle\langle k| - |l\rangle\langle l|), \quad (\text{A2})$$

with $\rho^{(k)} = \langle k|\rho|k\rangle$. To obtain the steady state, we solve $\partial\rho/\partial t = 0$, i.e.

$$\sum_{l=1}^{n-1} \sum_{k=0}^{l-1} C_{k,l} (|k\rangle\langle k| - |l\rangle\langle l|) = 0, \quad (\text{A3})$$

where $C_{k,l} = q_{k,l} \left(-\tau_{k,l}^e \rho^{(k)} + \tau_{k,l}^g \rho^{(l)} \right)$.

First, let us separate the equation into two terms as

$$\sum_{l=1}^{n-1} \sum_{k=0}^{l-1} C_{k,l} |k\rangle\langle k| - \sum_{l=1}^{n-1} \sum_{k=0}^{l-1} C_{k,l} |l\rangle\langle l| = 0. \quad (\text{A4})$$

The first term can be written in a different way,

$$\begin{aligned} \sum_{l=1}^{n-1} \sum_{k=0}^{l-1} C_{k,l} |k\rangle\langle k| &= \sum_{l=1}^{n-1} C_{0,l} |0\rangle\langle 0| + \sum_{l=2}^{n-1} C_{1,l} |1\rangle\langle 1| \\ &\quad + \cdots + \sum_{l=n-1}^{n-1} C_{n-2,l} |n-2\rangle\langle n-2| \\ &= \sum_{s=0}^{n-2} \sum_{l=s+1}^{n-1} C_{s,l} |s\rangle\langle s| \\ &= \sum_{l=1}^{n-1} C_{0,l} |0\rangle\langle 0| + \sum_{s=1}^{n-2} \sum_{l=s+1}^{n-1} C_{s,l} |s\rangle\langle s|, \quad (\text{A5}) \end{aligned}$$

and the second term can be written as

$$\sum_{l=1}^{n-1} \sum_{k=0}^{l-1} C_{k,l} |l\rangle\langle l| = \sum_{l=1}^{n-2} \sum_{k=0}^{l-1} C_{k,l} |l\rangle\langle l| + \sum_{k=0}^{n-2} C_{k,n-1} |n-1\rangle\langle n-1|. \quad (\text{A6})$$

Thus, the left hand side (l.h.s) of Eq. (A4) is rewritten as

$$\begin{aligned} \text{l.h.s of Eq. (A4)} &= \sum_{l=1}^{n-1} C_{0,l} |0\rangle\langle 0| - \sum_{k=0}^{n-2} C_{k,n-1} |n-1\rangle\langle n-1| \\ &\quad + \sum_{s=1}^{n-2} \sum_{l=s+1}^{n-1} C_{s,l} |s\rangle\langle s| - \sum_{l=1}^{n-2} \sum_{k=0}^{l-1} C_{k,l} |l\rangle\langle l| \\ &= \sum_{l=1}^{n-1} C_{0,l} |0\rangle\langle 0| - \sum_{k=0}^{n-2} C_{k,n-1} |n-1\rangle\langle n-1| \\ &\quad + \sum_{s=1}^{n-2} \left(\sum_{l=s+1}^{n-1} C_{s,l} - \sum_{k=0}^{s-1} C_{k,s} \right) |s\rangle\langle s|. \quad (\text{A7}) \end{aligned}$$

Since each of the terms in Eq. (A4) is zero, we can obtain n equations such as

$$\sum_{l=s+1}^{n-1} C_{s,l} - \sum_{k=0}^{s-1} C_{k,s} = 0, \text{ for } \{1 \leq k \leq n-2 : \forall k \in \mathbb{Z}\}, \quad (\text{A8a})$$

$$\sum_{l=1}^{n-1} C_{0,l} = 0, \quad (\text{A8b})$$

$$\sum_{k=0}^{n-2} C_{k,n-1} = 0. \quad (\text{A8c})$$

The above n equations can be written in a matrix form as

$$\mathbf{M}_n \vec{\rho}_{ss} = \vec{0} \quad (\text{A9})$$

where $\vec{\rho}_{ss} = (\rho_{ss}^{(0)}, \rho_{ss}^{(1)}, \dots, \rho_{ss}^{(n-1)})^T$ and \mathbf{M}_n is an $n \times n$ matrix given by

$$\mathbf{M} = \begin{pmatrix} M_{0,0} & q_{0,1}\tau_{0,1}^g & q_{0,2}\tau_{0,2}^g & \cdots & q_{0,n-2}\tau_{0,n-2}^g & q_{0,n-1}\tau_{0,n-1}^g \\ q_{0,1}\tau_{0,1}^e & M_{1,1} & q_{1,2}\tau_{1,2}^g & \cdots & q_{1,n-2}\tau_{1,n-2}^g & q_{1,n-1}\tau_{1,n-1}^g \\ q_{0,2}\tau_{0,2}^e & q_{1,2}\tau_{1,2}^e & \ddots & \ddots & \vdots & \vdots \\ \vdots & \vdots & & \ddots & \vdots & \vdots \\ q_{0,n-2}\tau_{0,n-2}^e & q_{1,n-2}\tau_{1,n-2}^e & \cdots & q_{n-3,n-2}\tau_{n-3,n-2}^e & M_{n-2,n-2} & q_{n-2,n-1}\tau_{n-2,n-1}^g \\ q_{0,n-1}\tau_{0,n-1}^e & q_{1,n-1}\tau_{1,n-1}^e & \cdots & q_{n-3,n-1}\tau_{n-3,n-1}^e & q_{n-2,n-1}\tau_{n-2,n-1}^e & M_{n-1,n-1} \end{pmatrix}. \quad (\text{A10})$$

The diagonal terms are given by

$$M_{0,0} = - \sum_{s=1}^{n-1} q_{0,s} \tau_{0,s}^e, \quad (\text{A11a})$$

$$M_{k,k} = - \left(\sum_{s=0}^{k-1} q_{s,k} \tau_{s,k}^g + \sum_{s=k+1}^{n-1} q_{k,s} \tau_{k,s}^e \right), \quad (\text{A11b})$$

$$M_{n-1,n-1} = - \sum_{s=0}^{n-2} q_{s,n-1} \tau_{s,n-1}^g \quad (\text{A11c})$$

for $1 \leq k \leq n-2$.

Here, we add the normalisation constraint, $\text{Tr}[\rho_{ss}] = 1$, into this simultaneous equation (A9), and hence the total number of equations involved in the simultaneous equation is $(n+1)$. However, the number of the variables in $\vec{\rho}_{ss}$ is n . This indicates that there is one excess equa-

tion in the simultaneous equation. In fact, any equation written in Eq. (A9) is dependent of other equations, (i.e. can be constructed from the rest of the equations). For example, the equation described by the first row in the matrix \mathbf{M} is reproduced by taking a sum of the equations

given by all other rows due to Eqs. (A11) and multiplying it by minus sign. Therefore, the removal of the first row from the matrix \mathbf{M} poses no problem for solving the simultaneous equation. We remove the first row and then add the normalisation constraint $\text{Tr}[\rho_{ss}] = 1$ as follows

$$\begin{aligned}
 \mathbf{M}_n \vec{\rho}_{ss} &= \begin{pmatrix} M_{0,0} & q_{0,1}\tau_{0,1}^g & q_{0,2}\tau_{0,2}^g & \cdots & q_{0,n-2}\tau_{0,n-2}^g & q_{0,n-1}\tau_{0,n-1}^g \\ q_{0,1}\tau_{0,1}^e & M_{1,1} & q_{1,2}\tau_{1,2}^g & \cdots & q_{1,n-2}\tau_{1,n-2}^g & q_{1,n-1}\tau_{1,n-1}^g \\ q_{0,2}\tau_{0,2}^e & q_{1,2}\tau_{1,2}^e & \ddots & \ddots & \vdots & \vdots \\ \vdots & \vdots & & & \vdots & \vdots \\ q_{0,n-2}\tau_{0,n-2}^e & q_{1,n-2}\tau_{1,n-2}^e & \cdots & q_{n-3,n-2}\tau_{n-3,n-2}^e & M_{n-2,n-2} & q_{n-2,n-1}\tau_{n-2,n-1}^g \\ q_{0,n-1}\tau_{0,n-1}^e & q_{1,n-1}\tau_{1,n-1}^e & \cdots & q_{n-3,n-1}\tau_{n-3,n-1}^e & q_{n-2,n-1}\tau_{n-2,n-1}^e & M_{n-1,n-1} \end{pmatrix} \begin{pmatrix} \rho_{ss}^{(0)} \\ \rho_{ss}^{(1)} \\ \vdots \\ \vdots \\ \rho_{ss}^{(n-1)} \end{pmatrix} \\
 &\rightarrow \begin{pmatrix} 0 & 0 & 0 & \cdots & 0 & 0 \\ q_{0,1}\tau_{0,1}^e & M_{1,1} & q_{1,2}\tau_{1,2}^g & \cdots & q_{1,n-2}\tau_{1,n-2}^g & q_{1,n-1}\tau_{1,n-1}^g \\ q_{0,2}\tau_{0,2}^e & q_{1,2}\tau_{1,2}^e & \ddots & \ddots & \vdots & \vdots \\ \vdots & \vdots & & & \vdots & \vdots \\ q_{0,n-2}\tau_{0,n-2}^e & q_{1,n-2}\tau_{1,n-2}^e & \cdots & q_{n-3,n-2}\tau_{n-3,n-2}^e & M_{n-2,n-2} & q_{n-2,n-1}\tau_{n-2,n-1}^g \\ q_{0,n-1}\tau_{0,n-1}^e & q_{1,n-1}\tau_{1,n-1}^e & \cdots & q_{n-3,n-1}\tau_{n-3,n-1}^e & q_{n-2,n-1}\tau_{n-2,n-1}^e & M_{n-1,n-1} \end{pmatrix} \begin{pmatrix} \rho_{ss}^{(0)} \\ \rho_{ss}^{(1)} \\ \vdots \\ \vdots \\ \rho_{ss}^{(n-1)} \end{pmatrix} \\
 &\rightarrow \begin{pmatrix} 1 & 1 & 1 & \cdots & 1 & 1 \\ q_{0,1}\tau_{0,1}^e & M_{1,1} & q_{1,2}\tau_{1,2}^g & \cdots & q_{1,n-2}\tau_{1,n-2}^g & q_{1,n-1}\tau_{1,n-1}^g \\ q_{0,2}\tau_{0,2}^e & q_{1,2}\tau_{1,2}^e & \ddots & \ddots & \vdots & \vdots \\ \vdots & \vdots & & & \vdots & \vdots \\ q_{0,n-2}\tau_{0,n-2}^e & q_{1,n-2}\tau_{1,n-2}^e & \cdots & q_{n-3,n-2}\tau_{n-3,n-2}^e & M_{n-2,n-2} & q_{n-2,n-1}\tau_{n-2,n-1}^g \\ q_{0,n-1}\tau_{0,n-1}^e & q_{1,n-1}\tau_{1,n-1}^e & \cdots & q_{n-3,n-1}\tau_{n-3,n-1}^e & q_{n-2,n-1}\tau_{n-2,n-1}^e & M_{n-1,n-1} \end{pmatrix} \begin{pmatrix} \rho_{ss}^{(0)} \\ \rho_{ss}^{(1)} \\ \vdots \\ \vdots \\ \rho_{ss}^{(n-1)} \end{pmatrix}. \quad (\text{A12})
 \end{aligned}$$

The full simultaneous equation turns to become

$$\mathbf{M} \begin{pmatrix} \rho_{ss}^{(0)} \\ \rho_{ss}^{(1)} \\ \vdots \\ \rho_{ss}^{(n-1)} \end{pmatrix} = \begin{pmatrix} 1 \\ 0 \\ \vdots \\ 0 \end{pmatrix}, \quad (\text{A13})$$

where the matrix \mathbf{M} is now redefined as

$$\mathbf{M} = \begin{pmatrix} 1 & 1 & 1 & \cdots & 1 & 1 \\ q_{0,1}\tau_{0,1}^e & M_{1,1} & q_{1,2}\tau_{1,2}^g & \cdots & q_{1,n-2}\tau_{1,n-2}^g & q_{1,n-1}\tau_{1,n-1}^g \\ q_{0,2}\tau_{0,2}^e & q_{1,2}\tau_{1,2}^e & \ddots & \ddots & \vdots & \vdots \\ \vdots & \vdots & & & \vdots & \vdots \\ q_{0,n-2}\tau_{0,n-2}^e & q_{1,n-2}\tau_{1,n-2}^e & \cdots & q_{n-3,n-2}\tau_{n-3,n-2}^e & M_{n-2,n-2} & q_{n-2,n-1}\tau_{n-2,n-1}^g \\ q_{0,n-1}\tau_{0,n-1}^e & q_{1,n-1}\tau_{1,n-1}^e & \cdots & q_{n-3,n-1}\tau_{n-3,n-1}^e & q_{n-2,n-1}\tau_{n-2,n-1}^e & M_{n-1,n-1} \end{pmatrix}. \quad (\text{A14})$$

Here, let us distinguish the two cases where the matrix \mathbf{M} is invertible and where it is not. In the latter case, the steady-state solution cannot be determined with the conditions we have. However, this issue can be avoided. For example, physically, this case corresponds to the case where one machine is coupled to the levels $|0\rangle$ and $|1\rangle$ in

a three-level system and the population ratios between the levels $|0\rangle$ and $|2\rangle$ and between the levels $|1\rangle$ and $|2\rangle$ are not determined. In this case, the steady state cannot be defined rigorously, and this leads to nonexistence of inverse matrix of \mathbf{M} . If one sees this three-level system as a two-level system composed of the levels $|0\rangle$ and $|1\rangle$,

the matrix \mathbf{M} can be rewritten as an invertible matrix.

Assuming that the matrix \mathbf{M} is invertible, the solution $\tilde{\rho}_{ss}$ is obtained as

$$\tilde{\rho}_{ss} = \mathbf{M}^{-1} \begin{pmatrix} 1 \\ 0 \\ \vdots \\ 0 \end{pmatrix}. \quad (\text{A15})$$

According to Cramer's rule, the inverse matrix can be written as

$$\mathbf{M}^{-1} = \frac{1}{\det[\mathbf{M}]} \text{adj}[\mathbf{M}], \quad (\text{A16})$$

where $\text{adj}[\mathbf{M}]$ is the adjugate of \mathbf{M} , given by $\text{adj}[\mathbf{M}] = [\{\Delta_{i,j}\}_{1 \leq i,j \leq n}]^T$, i.e.

$$\text{adj}[\mathbf{M}] = \begin{pmatrix} \Delta_{1,1} & \Delta_{2,1} & \cdots & \Delta_{n,1} \\ \Delta_{1,2} & \Delta_{2,2} & \cdots & \Delta_{n,2} \\ \vdots & \vdots & \ddots & \vdots \\ \Delta_{1,n} & \Delta_{2,n} & \cdots & \Delta_{n,n} \end{pmatrix}. \quad (\text{A17})$$

Here, $\Delta_{i,j}$ is a set of the cofactors of the matrix \mathbf{M} and defined as

$$\Delta_{i,j} = (-1)^{i+j} \begin{vmatrix} M_{0,0} & \cdots & M_{0,j-1} & M_{0,j+1} & \cdots & M_{0,n-1} \\ \vdots & \vdots & \vdots & \vdots & \vdots & \vdots \\ M_{i-1,0} & \cdots & M_{i-1,j-1} & M_{i-1,j+1} & \cdots & M_{i-1,n-1} \\ M_{i+1,0} & \cdots & M_{i+1,j-1} & M_{i+1,j+1} & \cdots & M_{i+1,n-1} \\ \vdots & \vdots & \vdots & \vdots & \vdots & \vdots \\ M_{n-1,0} & \cdots & M_{n-1,j-1} & M_{n-1,j+1} & \cdots & M_{n-1,n-1} \end{vmatrix}. \quad (\text{A18})$$

Also, due to the mathematical properties of the determinant, we get $\det[\mathbf{M}] = \sum_{s=1}^n \Delta_{1,s}$. As a results, the solution $\tilde{\rho}_{ss}$ is then written as

$$\tilde{\rho}_{ss} = \frac{1}{\sum_{s=1}^n \Delta_{1,s}} \begin{pmatrix} \Delta_{1,1} \\ \Delta_{1,2} \\ \vdots \\ \Delta_{1,n} \end{pmatrix}, \quad (\text{A19})$$

which is normalised as $\sum_{j=1}^n \rho_{ss}^{(j)} = 1$ with $\rho_{ss}^{(j)}$ being an element of the density matrix. For $n = 2$, the solution (A19) gives the thermal state of the virtual temperature, $\rho_{ss} = (\tau_{0,1}^g, \tau_{0,1}^e)^T$ as expected. For $n = 3$, the solution (A19) corresponds to Eq. (11). For the solution (A19) for $n = 4$, see the Appendix B.

Appendix B: Steady-state solution of effRME for four-level system

One can obtain the steady state of the effRME for any-level target system from Eq. (A19). In this appendix, we focus on a four-level target system and discuss components of its steady state. Let us recall that the steady state (11) of the effRME for qutrit target systems is combination of another steady states where two pairs of levels are characterised with different temperatures, weighted with the effective thermalisation rates q_i . Even for higher-level systems, the same feature can be seen as shown below.

Suppose that one has a four-level target system where each pair of levels are occupied by one two-qubit machine (in total six machines are involved). The steady-state solution of the effRME is given by

$$\begin{aligned} \frac{\rho_{ss}}{C} = & q_0^3 q_1^3 q_2^3 \tau_{012}^{333} \\ & + q_0^3 q_1^3 q_0^2 \tau_{010}^{332} + q_0^3 q_1^3 q_1^2 \tau_{011}^{332} \\ & + q_0^3 q_2^3 q_0^2 \tau_{020}^{331} + q_0^3 q_2^3 q_1^2 \tau_{021}^{332} \\ & + q_1^3 q_2^3 q_0^2 \tau_{120}^{331} + q_1^3 q_2^3 q_1^2 \tau_{120}^{332} \\ & + q_0^3 q_0^2 q_0^2 \tau_{000}^{312} + q_0^3 q_0^2 q_1^2 \tau_{001}^{312} + q_0^3 q_0^2 q_1^2 \tau_{001}^{322} \\ & + q_1^3 q_0^2 q_0^2 \tau_{100}^{312} + q_1^3 q_0^2 q_1^2 \tau_{101}^{312} + q_1^3 q_0^2 q_1^2 \tau_{101}^{322} \\ & + q_2^3 q_0^2 q_0^2 \tau_{200}^{312} + q_2^3 q_0^2 q_1^2 \tau_{201}^{312} + q_2^3 q_0^2 q_1^2 \tau_{201}^{322}, \end{aligned} \quad (\text{B1})$$

where the normalisation constant C is given by the trace of the right hand side of Eq. (B1). 16 states such as τ_{012}^{333} in the solution are steady states with three of the coherent couplings on. For example,

$$\begin{aligned} \tau_{012}^{333} = & \tau_{0,3}^g \tau_{1,3}^e \tau_{2,3}^e |0\rangle\langle 0| + \tau_{0,3}^e \tau_{1,3}^g \tau_{2,3}^e |1\rangle\langle 1| \\ & + \tau_{0,3}^g \tau_{1,3}^e \tau_{2,3}^g |2\rangle\langle 2| + \tau_{0,3}^e \tau_{1,3}^g \tau_{2,3}^g |3\rangle\langle 3|, \end{aligned} \quad (\text{B2})$$

which is not normalised on purpose, such as Eq. (12). In this state, three pairs of the levels are characterised with different virtual temperatures.

The steady-state solution (B1) consists of 16 steady states where three of the coherent couplings are present in the system (e.g. τ_{012}^{333}). However, notice that the solution (B1) does not cover all the possible steady states with three of the couplings on. For example, a case is excluded where three two-qubit machines are coupled to the transitions between $|0\rangle$ and $|1\rangle$, between $|0\rangle$ and $|3\rangle$, and between $|1\rangle$ and $|3\rangle$. There are some differences between the excluded cases and the included cases. In the excluded cases, one level is unoccupied. For the above example, the level $|2\rangle$ is free. Moreover, the excluded cases are essentially the same as the situation depicted in Fig. 2, i.e. the three thermalisation processes compete. As discussed in Sec. III.1, this kind of steady states cannot be simply described with just the virtual temperature, but effective rates are required in contrast to Eq. (B2). In brief, the steady state (B1) is composed of another steady states that coherently interact with three machines and where the thermalisation processes caused by their machines do not compete against each other.